

Full length article



# Excess thermochemical properties and local structure in the entropy stabilized (Hf-Zr)TiO<sub>4</sub> system

William Rosenberg<sup>a</sup>, Stuart C. Ness<sup>a</sup>, Bhoopesh Mishra<sup>b</sup>, Carlo U. Segre<sup>b</sup>,  
Scott J. McCormack<sup>c,\*</sup>

<sup>a</sup> Department of Chemical Engineering, University of California, Davis, Davis, CA 95616, United States

<sup>b</sup> Department of Physics & CSRRI, Illinois Institute of Technology, Chicago, IL 60616, United States

<sup>c</sup> Department of Materials Science and Engineering, University of California, Davis, Davis, CA 95616, United States

## ARTICLE INFO

### Keywords:

Entropy-stabilized oxides  
Calorimetry  
Non-ideal mixing  
X-ray diffraction  
X-ray absorption spectroscopy  
Local structure  
Crystallography

## ABSTRACT

To study non-ideal mixing in an entropy stabilized system, the entropy stabilized oxides HfTiO<sub>4</sub> and ZrTiO<sub>4</sub> were mixed to form the single phase (Hf-Zr)TiO<sub>4</sub> system. HfTiO<sub>4</sub> and ZrTiO<sub>4</sub> are entropy stabilized relative to their constituent oxides (HfO<sub>2</sub>, ZrO<sub>2</sub>, and TiO<sub>2</sub>). Oxide-melt solution calorimetry (OSMC) was performed to determine enthalpies of formation relative to the constituent oxides ( $\Delta H_{f,ox}$ ) for 11 compositions in the (Hf-Zr)TiO<sub>4</sub> system.  $\Delta H_{f,ox}$  for HfTiO<sub>4</sub> was determined to be  $22.81 \pm 2.61$  kJ/mol.  $\Delta H_{f,ox}$  for ZrTiO<sub>4</sub> was measured to be  $20.79 \pm 2.67$  kJ/mol which is in good agreement with literature values. Positive  $\Delta H_{f,ox}$  values for HfTiO<sub>4</sub> and ZrTiO<sub>4</sub> demonstrates entropy stabilization. X-ray absorption spectroscopy (XAS) data shows that Ti is locally segregated from the Hf and Zr.  $\Delta H_{f,ox}$  values for mixed HfTiO<sub>4</sub>-ZrTiO<sub>4</sub> samples were used to calculate enthalpies of mixing relative to the HfTiO<sub>4</sub> and ZrTiO<sub>4</sub> end points ( $\Delta H_{mix}$ ).  $\Delta H_{mix}$  was determined to be most exothermic ( $\Delta H_{mix} = -5.3$  kJ/mol) at a composition of (Hf<sub>0.5</sub>Zr<sub>0.5</sub>)TiO<sub>4</sub>. Negative  $\Delta H_{mix}$  suggests that Hf and Zr experience further ordering upon mixing of HfTiO<sub>4</sub> and ZrTiO<sub>4</sub>. X-ray powder diffraction (XRPD) experiments show that the (Hf-Zr)TiO<sub>4</sub> system forms a single-phase product across the composition range with pbcn symmetry (space group #60) and does not form any ordered super structures, as noted by the lack of superlattice reflections. X-ray powder diffraction (XRPD) data additionally reveals that the (Hf-Zr)TiO<sub>4</sub> system has a highly anisotropic positive excess volume, with the majority of the excess volume resulting from changes in the b-lattice parameter. X-ray absorption spectroscopy (XAS) results demonstrate that mixing between Hf and Zr on the local level is non-ideal but cannot ascertain if ordering or segregation occurs. High-resolution transmission electron microscopy (HR-TEM) experiments are needed to fully elucidate the local structure in the (Hf-Zr)TiO<sub>4</sub> system. Using the (Hf-Zr)TiO<sub>4</sub> system as case study, this work shows that mixing in entropy stabilized systems is not always ideal and can give rise to complex local structures that can have interesting and unexpected effects on the chemical and physical properties, such as the large excess expansion along the b-direction.

## 1. Introduction

### 1.1. Entropy stabilized systems

In recent years there has been much excitement surrounding the fields of high entropy alloys (HEAs) [1–4], high entropy ceramics (HECs) [5], and high entropy oxides (HEOs) [6–14]. These compounds include compositionally diverse and highly tunable materials, providing vast potential for utility in several technological applications. High entropy ceramics are typically considered to have 5 or more components,

resulting in a maximum ideal configurational entropy of 1.6079R [1–4]. In ‘high entropy’ systems, it is expected that non-ideal mixing effects will reduce the configurational entropy from this ideal value and could lead to interesting and unexpected properties. The criteria defining ‘high entropy’ ceramics is largely arbitrary, and it has been demonstrated that systems with as few as two components can form a single-phase compound that is stabilized through entropic effects above a certain transition temperature,  $T_{trans}$  [14]. Thus, multi-component single-phase ceramics, regardless of number of components, that are stabilized through entropic effects have been aptly named ‘entropy stabilized

\* Corresponding author.

E-mail address: [sjmccormack@ucdavis.edu](mailto:sjmccormack@ucdavis.edu) (S.J. McCormack).

<https://doi.org/10.1016/j.actamat.2024.120639>

Received 24 June 2024; Received in revised form 2 December 2024; Accepted 7 December 2024

Available online 9 December 2024

1359-6454/© 2024 The Authors. Published by Elsevier Ltd on behalf of Acta Materialia Inc. This is an open access article under the CC BY license (<http://creativecommons.org/licenses/by/4.0/>).

ceramics [14]. At the transition temperature, the entropic term overcomes a positive enthalpic term, leading to a negative Gibb's free energy of formation (Eq. (1)). In such chemical systems, Gibb's free energy of formation is an indicator of chemical stability. For example, the five component rocksalt oxide synthesized by Rost et al. [15–17] with MO stoichiometry ( $M = \text{Mg, Ni, Co, Zn, Cu}$ ) has exhibited reversible endothermic formation from the binary oxides and has existed as a test case for entropy stabilized oxides.

$$\Delta G_f = \Delta H_f - T\Delta S_f \quad (1)$$

Eq. (1): Gibb's Free Energy of Formation as a function of the enthalpy of formation ( $\Delta H_f$ ), the entropy of formation ( $\Delta S_f$ ), and temperature ( $T$ ).

In chemical systems it is thermodynamically preferred to minimize Gibb's Free energy. In a formation reaction, a positive  $\Delta G_f$  indicates that reactants will dominate, rather than products. Thus, if a compound has a positive  $\Delta H_f$ , the reactants will be favored unless there is sufficient  $T\Delta S_f$  to drive  $\Delta G_f$  below 0. With that in mind, if an endothermic reaction has a  $T\Delta S_f > \Delta H_f$ , the compound is said to be entropy stabilized with respect to its components. It should be noted that as the entropic term scales with temperature, there will exist some critical temperature where the entropic contribution will not be large enough to overcome the positive  $\Delta H_f$ , and reactants will be favored [18,19].

Much work has been done to highlight properties in entropy stabilized oxides [20], but the thermodynamics of mixing in these systems are often simplified by assuming that mixing in entropy stabilized systems is ideal. In mixed systems, the presence of excess thermochemical properties such as enthalpy and molar volume, are evidence of non-ideal mixing [21,22]. For example, a positive mixing enthalpy destabilizes the system by increasing Gibb's free energy and implies chemical segregation in the local structure or phase separation through a miscibility gap if temperature is insufficient. A negative enthalpy of mixing further stabilizes the system by lowering the Gibb's free energy, and implies ordering in the local structure, which if large enough can lead to a change in symmetry from long range ordering of atoms. In many real oxide systems, the enthalpy of mixing is not negligible [14], and assuming ideal mixing neglects the importance of unique, non-ideal, structural and chemical interactions that can have a substantial effect on material properties. Unfortunately, enthalpy of mixing data is scarce in entropy stabilized systems. To understand the importance of non-ideal mixing in an entropy stabilized oxide, enthalpies of mixing, excess volume, and local-structure were examined using the (Hf-Zr)TiO<sub>4</sub> system as a case study.

## 1.2. The (Hf-Zr)TiO<sub>4</sub> system

HfTiO<sub>4</sub> and ZrTiO<sub>4</sub> are both orthorhombic, pbcn symmetry (space group #60) [23–27],  $\alpha$ -PbO<sub>2</sub> derived structures [28], entropy stabilized oxides, that are well known as low thermal expansion [29–37], bulk refractory ceramics [38–45]. Most research on HfTiO<sub>4</sub> and ZrTiO<sub>4</sub> has historically been focused on electrical properties and utility as high-k microwave dielectric materials in telecommunications applications [39–45]. Lopez-Lopez et al. additionally studied the thermomechanical properties of ZrTiO<sub>4</sub> to assess its potential for use in thermal shock applications [46]. Local structure and ordering in ZrTiO<sub>4</sub> has also been examined in various studies using high resolution transmission electron microscopy (HR-TEM) and single crystal electron diffraction experiments [47–55]. Studies have shown that Zr and Ti segregate on the local scale in bulk disordered ZrTiO<sub>4</sub> compounds. A more in-depth discussion of local structures in ZrTiO<sub>4</sub> is provided in Section 3.4. To date, no local structure studies have been published on HfTiO<sub>4</sub>, as recent work on HfTiO<sub>4</sub> has been focused on its electrical properties and the manufacture of thin films through various deposition techniques [54–56]. With that said, HfTiO<sub>4</sub> and ZrTiO<sub>4</sub> are isomorphic, and thus it is expected that similar structural features would be observed.

As demonstrated by the endothermic polyphase to single phase

transition, ZrTiO<sub>4</sub> [57] and HfTiO<sub>4</sub> (this work) have a positive  $\Delta H_{f,ox}$  at 298 K and are entropy stabilized with respect to the constituent oxides (TiO<sub>2</sub>, ZrO<sub>2</sub> and HfO<sub>2</sub>) (Eq. (5), Eq. (6)). While HfTiO<sub>4</sub> and ZrTiO<sub>4</sub> are entropy stabilized, they do not have large enough  $\Delta S_{config}$  to be considered 'high entropy' by the typical  $n \geq 5$  or  $\Delta S_{config} \geq 1.6079R$  criteria [58].



Eq. (5): Formation reaction of ATiO<sub>4</sub> from the constituent oxides (AO<sub>2</sub>, TiO<sub>2</sub>). A = Hf, Zr.

$$\Delta G_{f,ox} = \Delta H_{f,ox} - T\Delta S_{f,ox} \quad (6)$$

Eq. (6): Gibb's free energy of formation for the formation of ATiO<sub>4</sub> compounds from their constituent oxides.  $\Delta H_{f,ox}$  is formation enthalpy relative the constituent oxides,  $\Delta S_{f,ox}$  is formation entropy relative to constituent oxides, and T is temperature.

To study the ZrTiO<sub>4</sub> low temperature regime and gain a full understanding of the entropy of the system, Hom et al. measured the heat capacity from near 0 K up to room temperature [57]. It has been shown through X-ray powder diffraction (XRPD) that HfTiO<sub>4</sub> and ZrTiO<sub>4</sub> both form a single-phase structure upon heat treatment at 1300 °C. Thus, there exists some transition temperature where  $T\Delta S_{f,ox} > \Delta H_{f,ox}$  for the (Hf-Zr)TiO<sub>4</sub> system that marks polyphase to single phase transition. A phase decomposition temperature of  $T = 1250 \pm 150K$  has been determined for ZrTiO<sub>4</sub> [57], demonstrating that the compound is stabilized through entropic contributions that scale with temperature.

HfTiO<sub>4</sub> and ZrTiO<sub>4</sub> are isomorphic, suggesting that mixing the compounds will yield a single-phase solid solution (Fig. 1). It is important to highlight the distinction between "ideal solid solutions" and "non-ideal solid solutions". An ideal solid solution is one in which the mixing properties are purely entropic as the local structure is perfectly random. A non-ideal solid solution is one in which the mixing properties incorporate non-ideal effects such as excess enthalpy, excess volume, etc., as the local structure is not perfectly random. Examples of non-ideal solid solutions in mixed oxide systems include: ZrO<sub>2</sub>-Y<sub>2</sub>O<sub>3</sub> [59], HfO<sub>2</sub>-Y<sub>2</sub>O<sub>3</sub> [60], CeO<sub>2</sub>-Y<sub>2</sub>O<sub>3</sub> [61], Y(Mn-In)O<sub>3</sub> [62], rare-earth titanate pyrochlores [63], and Mg<sub>1-x</sub>Ni<sub>x</sub>Al<sub>2</sub>O<sub>4</sub> spinel [64].

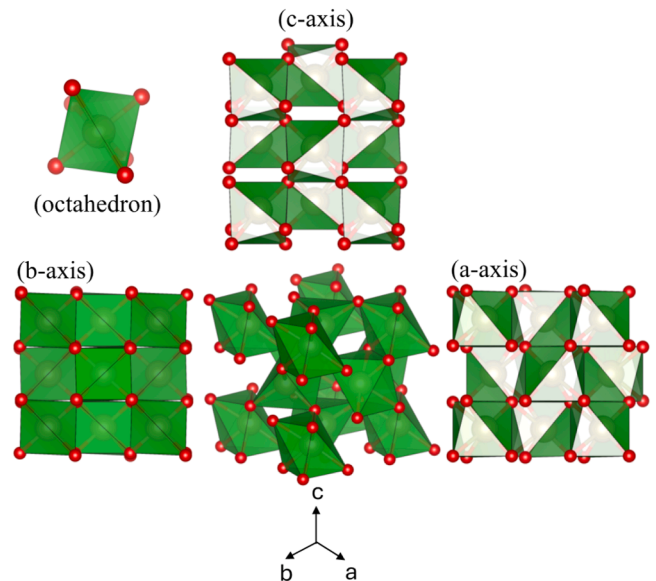


Fig. 1. Disordered crystal structure of (Hf<sub>0.5</sub>Zr<sub>0.5</sub>)TiO<sub>4</sub> visualized using VESTA. Model was generated from X-Ray powder diffraction data of (Hf<sub>0.5</sub>Zr<sub>0.5</sub>)TiO<sub>4</sub>. The space group is Pbcn and in the disordered model, Ti, Zr, Hf atoms are sitting on the same sites and are coordinated with 6 oxygens to form distorted octahedra. The octahedra exhibit both corner and edge sharing in the structure. The number of formula units per unit cell (Z) is 4.

To understand the effect of mixing when mixing two entropy stabilized oxides, this study will measure (i) the enthalpy of mixing between  $\text{HfTiO}_4$  and  $\text{ZrTiO}_4$  via oxide-melt solution calorimetry (OSMC), (ii) the excess volume of mixing between  $\text{HfTiO}_4$  and  $\text{ZrTiO}_4$  through X-ray powder diffraction (XRPD) and (iii) perform X-ray absorption spectroscopy (XAS) to probe the atomic local structure to understand how Ti, Zr and Hf are coordinating within the single phase, entropy stabilized (Hf-Zr)TiO<sub>4</sub> system.

## 2. Methods

### 2.1. Synthesis

All compositions in the (Hf-Zr)TiO<sub>4</sub> system were synthesized using the steric entrapment method [65–67].  $\text{HfCl}_4$  (99.9%, Sigma Millipore) and  $\text{ZrCl}_4$  (99.99%, Sigma Millipore) were measured out in varying Hf:Zr ratios. Once weighed out,  $\text{HfCl}_4$  and  $\text{ZrCl}_4$  were stirred in 50 mL of DI water until completely dissolved. Titanium isopropoxide (99.9% Sigma Millipore), also known as  $\text{Ti}(\text{iSO})_4$ , was calibrated and dissolved in 80 mL isopropyl alcohol (HPLC grade, Sigma Millipore). The  $\text{HfCl}_4$ ,  $\text{ZrCl}_4$ , and  $\text{Ti}(\text{iSO})_4$  solutions were mixed and allowed to homogenize. Once homogenized, Ethylene Glycol (99.8%, Sigma Millipore) was added to the mixture in a 4:1 cation valence to  $\text{OH}^-$  ratio and continuously stirred. The ethylene glycol,  $\text{HfCl}_4$ ,  $\text{ZrCl}_4$ , and  $\text{Ti}(\text{iSO})_4$  mixture was heated on a hotplate set to 300 °C and stirred continuously until reduced to a clear gel. The gel was dried in a vented box furnace set to 450 °C for 12 h (Heated 5 °C/min, Cooled 5 °C/min). Product was obtained as a flaky brown powder. Product was ground in a Ytria-Stabilized Zirconia (YSZ) mortar and pestle and calcined in a lidded YSZ crucible at 1000 °C for 12 h (Heated 5 °C/min, Cooled 5 °C/min) in air. Product was obtained as a shiny white powder. The powder was pressed into a 22 mm pellet at 155 MPa in an MTI cold uniaxial hydraulic press. The pellet was then annealed in a lidded YSZ crucible at 1300 °C for 12 h (Heated 5 °C/min, Cooled 5 °C/min) in air. The annealed pellet was ground into the final product, a fine white powder, in an YSZ mortar and pestle.

### 2.2. X-ray diffraction and volume measurements

XRPD measurements were performed using the synchrotron source at the 11-BM beamline at Argonne National Laboratory's Advanced Photon Source. The 11-BM program only accepts proposals for up to eight compounds, so synchrotron XRPD data is unavailable for compositions  $(\text{Hf}_{.3}\text{Zr}_{.7})\text{TiO}_4$ ,  $(\text{Hf}_{.7}\text{Zr}_{.3})\text{TiO}_4$ , and  $(\text{Hf}_{.9}\text{Zr}_{.1})\text{TiO}_4$ . Compounds with even Hf-Zr stoichiometry were selected to maintain an even trend in the data. The midpoint,  $\text{Hf}_{.5}\text{Zr}_{.5}\text{TiO}_4$  was selected due to it being the composition where the magnitude of mixing enthalpy is maximized.  $\text{Hf}_{.1}\text{Zr}_{.9}\text{TiO}_4$  was selected to improve data resolution in the Zr rich compositions.

Rietveld refinement [68] was performed on XRPD patterns using the computer program GSAS-II [69] to confirm product purity and generate crystallographic information files (CIFs) at each composition. GSAS-II refinement files and the generated CIFs can be found in Supplementary Information S1 and S2, respectively. From these CIFs, unit cell volume and lattice parameters were obtained. Cation stoichiometry was confirmed using a Rigaku SuperMini200 X-ray Fluorescence Spectrometer (XRF) Eq. uipped with  $\text{LiF}(200)$ , PET, and RX25 crystals. Samples were loaded in boric acid substrate shells (5 mm, Vprep Corp). XRF measurements are included in the Supplementary Information S3.

### 2.3. Calorimetry measurements

Calorimetry of (Hf-Zr)TiO<sub>4</sub> samples was performed on a Twin-Calvet high temperature oxide melt calorimeter at 700 °C with sodium molybdate ( $3\text{Na}_2\text{O}\cdot 4\text{MoO}_3$ ) as the solvent. Oxide-melt calorimetry and its applications for determining formation enthalpies for oxides has been studied extensively by Navrotsky et al. [70–72]. Additionally,  $\Delta H_{f,ox}$  for

$\text{ZrTiO}_4$  has been previously determined through oxide-melt calorimetry at 700 °C [57]. Thus, oxide-melt calorimetry was deemed a suitable method to determine  $\Delta H_{f,ox}$  values for the (Hf-Zr)TiO<sub>4</sub> system. 20 g of solvent per drop-tube was weighed and melted in platinum crucibles in a can furnace at 800 °C. Once melted and allowed to cool, solvent and platinum crucibles were transferred into the Twin-Calvet calorimeter and allowed to heat to 700 °C overnight.

Air was flushed through the setup via platinum bubbling tubes to ensure that solvent was well mixed and to increase dissolution rates. (Hf-Zr)TiO<sub>4</sub> was pressed into pellets in a mass range of 5 mg - 30 mg. Pellet mass vs drop solution enthalpy ( $\Delta H_{ds}$ ) is plotted in Supplementary Information S4 to demonstrate that pellets are dissolving fully, where  $\Delta H_{ds}$  is the change in enthalpy generated by dropping a room temperature sample into the oxide melt, per mole of sample. Pellets were dropped on alternating sides of the calorimeter until a minimum of eight data points were obtained. Average dissolution time was 30 min. New solvent was used for every composition in the (Hf-Zr)TiO<sub>4</sub> system to ensure a dilute solvent.

Calibration for endothermic samples such as oxides was performed by dropping sapphire or platinum in known masses and recording the resulting heat affect. The sapphire calibration factor is used for endothermic samples with small heat effects and the platinum calibration factor is used for high heat-effect samples. (Hf-Zr)TiO<sub>4</sub> calorimetry samples were prepared in the mass range of 5–25 mg, so the sapphire calibration factor was used for the (Hf-Zr)TiO<sub>4</sub> system. As the oxide-melt calorimeters are twin calorimeters, each side needed to be calibrated individually. Calibration factors of  $-0.004700994120 \text{ J}/\mu\text{V}\cdot\text{s}$  and  $0.004677933 \text{ J}/\mu\text{V}\cdot\text{s}$  were determined for the used calorimeter. It should be noted that each side of the calorimeter is reverse wired. As a result, voltage readouts from the calorimeter's two sides have opposite signs, leading to calibration factors having opposite signs. Raw data for all calorimetry drops in this work can be found in Supplementary Information S5.

### 2.4. X-ray absorption spectroscopy

X-ray absorption spectroscopy measurements were taken for the Ti (4965 eV) and Zr (17,996 eV) K-edges and the Hf L<sub>3</sub>-edge (9558 eV) using the Materials Research Collaborative Access Team (MRCAT) bending magnet beamline, 10-BM-B at Argonne National Laboratory's Advanced Photon Source [73]. Powder samples were prepared in pellets using boron nitride as a filler and polyvinylidene fluoride (PVDF) as a binder and measured in transmission for the Zr and Hf edges and in fluorescence using a 5-grid fluorescence detector for the Ti edge. Multiple data sets were collected for each edge in continuous scan mode, rebinned, merged, normalized, background subtracted and fitted using the IFEFFIT-based Athena and Artemis programs [74,75]. The data ranges used for the Fourier Transform of the  $\chi(k)$  EXAFS data were  $2.2 < k < 7.5 \text{ \AA}^{-1}$ ,  $2.0 < k < 12 \text{ \AA}^{-1}$ ,  $3.0 < k < 11.0 \text{ \AA}^{-1}$  for the Ti, Zr, and Hf edges, respectively. All Fourier Transforms were processed with a Hanning window function with  $dk = 2.0 \text{ \AA}^{-1}$  for Zr and Hf and  $dk = 1.0 \text{ \AA}^{-1}$  for Ti. The Fourier Transform  $\chi(R)$  spectra were fitted over the range  $1.0 < R < 3.0 \text{ \AA}$ ,  $1.0 < R < 3.0 \text{ \AA}$   $1.0 < R < 4.0 \text{ \AA}$  and  $1.0 < R < 3.8 \text{ \AA}$  for Ti, Zr, and Hf edges, respectively. Lower  $\chi^2$  (reduced chi square) was used as the criterion for inclusion of an additional single-scattering paths in a path-by-path EXAFS fitting approach. Due to limited data ranges, all Ti edges were modelled simultaneously only with the nearest neighbour Ti-O scattering paths using common Ti-O bond lengths and disorder parameters,  $\sigma^2$  (Supplementary Information S8). The EXAFS of only the endpoint compositions,  $\text{ZrTiO}_4$  for Zr and  $\text{HfTiO}_4$  for Hf, were modelled.

### 3. Results and discussion

#### 3.1. Enthalpy of mixing

Drop solution enthalpies ( $\Delta H_{ds}$ ) at 700 °C were measured for 11 compounds in the (Hf-Zr)TiO<sub>4</sub> system.  $\Delta H_{ds}$  (Eq. (6)) has a component that accounts for the heat effects of raising the sample from room temperature to the calorimeter's operating temperature ( $\Delta H_{heat}$ ) as well as the heat of dissolution of the sample ( $\Delta H_{diss}$ ) (Eq. (1)) [50–52].

$$\Delta H_{ds} = \Delta H_{heat} + \Delta H_{diss} \quad (7)$$

Eq. (7): Drop solution enthalpy as recorded by Twin-Calvet high temperature oxide melt drop solution calorimeters.  $\Delta H_{heat}$  is the energy required to heat a sample in the calorimeter, it is equal to the integral of the heat capacity of the material across the specified temperature range.  $\Delta H_{diss}$  is the heat of dissolution of the specified sample.

$\Delta H_{heat}$  is a function of heat capacity and is determined through calibration of the calorimeters. Calibration of calorimeters is done to convert a voltage produced across the thermopile into heat. Once  $\Delta H_{heat}$  has been accounted for, the remaining term  $\Delta H_{diss}$ , is a representation of the energy required to dissolve the compound into solution.

Enthalpies of formation ( $\Delta H_{f,ox}$ ) from the constituent oxides, TiO<sub>2</sub>, ZrO<sub>2</sub>, and HfO<sub>2</sub>, were calculated by applying Hess's law to the  $\Delta H_{ds}$  data obtained through oxide-melt calorimetry. The thermocycles used to calculate  $\Delta H_{f,ox}$  are shown in Table 1. Hess's law calculations are normalized to 1 mole of TiO<sub>2</sub>. The behavior of the sodium molybdate (3Na<sub>2</sub>O\*4MoO<sub>3</sub>) melt has been studied extensively [72]. Mixing enthalpies were determined by subtracting the measured  $\Delta H_{f,ox}$  of mid points in the (Hf-Zr)TiO<sub>4</sub> system from the ideal mixing calculated from a linear combination of the endpoints (HfTiO<sub>4</sub> and ZrTiO<sub>4</sub>) (Eqs. (8), (9)).

$$\Delta H_{ideal\ mixing}^{x_1 HfTiO_4 + x_2 ZrTiO_4} = x_1 \Delta H_{f,ox,measured}^{HfTiO_4} + x_2 \Delta H_{f,ox,measured}^{ZrTiO_4} \quad (8)$$

Eq. (8): Calculation of ideal mixing in the (Hf-Zr)TiO<sub>4</sub> system (i.e. excess enthalpy is zero).  $x_1$  is the mole fraction of HfTiO<sub>4</sub> and  $x_2$  is the mole fraction of ZrTiO<sub>4</sub>.  $\Delta H_{f,ox,measured}^{HfTiO_4}$  and  $\Delta H_{f,ox,measured}^{ZrTiO_4}$  are the  $\Delta H_{f,ox}$  values of the endpoints as determined through oxide-melt calorimetry.

$$\Delta H_{mix}^{(Hf_{x_1}Zr_{x_2})TiO_4} = \Delta H_{f,ox,measured}^{(Hf_{x_1}Zr_{x_2})TiO_4} - \Delta H_{ideal\ mixing}^{x_1 HfTiO_4 + x_2 ZrTiO_4} \quad (9)$$

Eq. (9): Calculation of  $\Delta H_{mix}$  for any composition in the (Hf-Zr)TiO<sub>4</sub> system.  $x_1$  is the mole fraction of HfTiO<sub>4</sub> and  $x_2$  is the mole fraction of ZrTiO<sub>4</sub>.  $\Delta H_{f,ox,measured}^{HfTiO_4}$  and  $\Delta H_{f,ox,measured}^{ZrTiO_4}$  are the  $\Delta H_{f,ox}$  values of the endpoints as determined through oxide-melt calorimetry.

$\Delta H_{f,ox}$  and  $\Delta H_{mix}$  are shown graphically in Fig. 2, as well as error bars for the calorimetric measurements. Error bars represent two times the

**Table 1**

Thermocycles used to calculate enthalpy of formation from constituent oxides (cycle 1) and enthalpy of formation from standard state components (Cycle 2) for oxide-melt calorimetry at 700 °C. *a* = measured in this work and presented in Supplementary Information S6. *b* = values from Refs. [76,77].

Reactions in Thermocycle	$\Delta H$ (kJ/mol)
Cycle 1: Enthalpy of formation from oxides	
$Hf_{x_1}Zr_{x_2}TiO_{4(s,298\ K)} \rightarrow x_1 HfO_{2(sln,973\ K)} + x_2 ZrO_2$ ( <sub>(sln,973 K) + TiO<sub>2</sub>(sln,973 K)</sub> )	$\Delta H_1 = \Delta H_{ds}$
$HfO_{2(s,298\ K)} \rightarrow HfO_{2(sln,973\ K)}$	$\Delta H_2$
$ZrO_{2(s,298\ K)} \rightarrow ZrO_{2(sln,973\ K)}$	$\Delta H_3$
$TiO_{2(s,298\ K)} \rightarrow TiO_{2(sln,973\ K)}$	$\Delta H_4$
$x_1 HfO_{2(s,298\ K)} + x_2 ZrO_{2(s,298\ K)} + TiO_{2(s,298\ K)} \rightarrow$ $Hf_{x_1}Zr_{x_2}TiO_{4(s,298\ K)}$	$\Delta H_{f,ox} = x_1 \Delta H_2 + x_2 \Delta H_3 +$ $\Delta H_4 - \Delta H_1$
Cycle 2: Enthalpy of formation from elements	
$Hf_{(s,298\ K)} + O_{2(g,298\ K)} \rightarrow HfO_{2(s,298\ K)}$	$\Delta H_5$
$Zr_{(s,298\ K)} + O_{2(g,298\ K)} \rightarrow ZrO_{2(s,298\ K)}$	$\Delta H_6$
$Ti_{(s,298\ K)} + O_{2(g,298\ K)} \rightarrow TiO_{2(s,298\ K)}$	$\Delta H_7$
$x_1 Hf_{(s,298\ K)} + x_2 Zr_{(s,298\ K)} + Ti_{(s,298\ K)} + 2 O_2 \rightarrow$ $Hf_{x_1}Zr_{x_2}TiO_{4(s,298\ K)}$	$\Delta H_{f,el} = x_1 \Delta H_5 + x_2 \Delta H_6 +$ $\Delta H_7 + \Delta H_{f,ox}$

standard error of the calorimetric measurements ( $\frac{\sigma}{\sqrt{N}}$  where  $\sigma$  is the standard deviation and  $N$  is the number of measurements). Values shown on the graph are tabulated in S6.

All members of the (Hf-Zr)TiO<sub>4</sub> system have a positive enthalpy of formation with respect to the component oxides (HfO<sub>2</sub>, ZrO<sub>2</sub>, TiO<sub>2</sub>). This emphasizes that the polyphase to single-phase transition is entropy-driven at a sufficient temperature. As visible in the phase diagrams, the composition range where the ATiO<sub>4</sub> phase forms ( $A = Hf, Zr$ ) is rather narrow, spanning mole fractions of approximately 0.45–0.6 TiO<sub>2</sub> in AO<sub>2</sub> [35,46]. A formal study into the enthalpy of mixing across the ATiO<sub>4</sub> single-phase region has not yet been performed, but  $\Delta H_{f,ox}$  for HfTiO<sub>4</sub> and for ZrTiO<sub>4</sub> at the 1:1 points respectively was determined to be positive.  $\Delta H_{f,ox}$  for both HfTiO<sub>4</sub> and ZrTiO<sub>4</sub> are shown in Table 2.

Measurements show that mixing enthalpy in (Hf-Zr)TiO<sub>4</sub> with respect to the HfTiO<sub>4</sub> and ZrTiO<sub>4</sub> end points is negative. A minimum  $\Delta H_{mix}$  for the (Hf-Zr)TiO<sub>4</sub> system of  $-5.3$  kJ/mol was recorded at a composition (Hf<sub>0.5</sub>Zr<sub>0.5</sub>)TiO<sub>4</sub>. Negative  $\Delta H_{mix}$  values show that mixing between HfTiO<sub>4</sub> and ZrTiO<sub>4</sub> is more enthalpically stable than would be expected for the ideal mixture (i.e. excess enthalpy of mixing is zero), and that mixing is non-ideal. This is visualized in Fig. 3. The result is that mixing in the (Hf-Zr)TiO<sub>4</sub> system is favorable with respect to the HfTiO<sub>4</sub> and ZrTiO<sub>4</sub> end points. As  $\Delta H_{f,ox}$  for all (Hf-Zr)TiO<sub>4</sub> compounds is positive, it important to recall that the system is still entropy stabilized with respect to the constituent oxides TiO<sub>2</sub>, ZrO<sub>2</sub> and HfO<sub>2</sub>.

$\Delta H_{mix}$  data for the (Hf-Zr)TiO<sub>4</sub> system was fit using the sub-regular solution model [78] (Eq. (10)). In a binary or pseudo-binary system, such as (Hf-Zr)TiO<sub>4</sub>, the key difference between the regular and sub-regular solution models is that the regular solution model assumes interaction parameters to be identical. For the sub-regular solution model,  $A \neq B$ , where  $A$  and  $B$  are interaction parameters determined through fitting. The result is that the sub regular solution model is better at fitting datasets that are asymmetrical. Upon observing Fig. 2, it can be noted the maximum of the magnitude of the mixing enthalpy is not centered on the midpoint but shifted towards the ZrTiO<sub>4</sub> rich compounds.

$$\Delta H_{mix} = A_H x_1^2 x_2 + B_H x_1 x_2^2 \quad (10)$$

Eq. (10): Sub-Regular Solution for excess enthalpy.  $A_H$  and  $B_H$  are sub-regular solution fitting parameters.  $x_1$  corresponds to ZrTiO<sub>4</sub> mole fraction and  $x_2$  corresponds to HfTiO<sub>4</sub> mole fraction. Fit parameters and statistics are tabulated in S6 of supplemental info.

To understand the role of enthalpy in the stabilization of the (Hf-Zr)TiO<sub>4</sub> system,  $\Delta H_{mix}$  can be compared with ideal configurational entropy. This relationship between enthalpy, entropy, and Gibb's free energy is shown in Eq. (1). For the (Hf<sub>0.5</sub>Zr<sub>0.5</sub>)TiO<sub>4</sub> midpoint,  $\Delta H_{mix}$  was determined to be  $-5.3$  kJ/mol. At this same composition, there is an ideal configurational entropy of  $1.04R$ . It must be made clear that this is the maximum possible value under the ideal mixing assumption, and as noted by the observed non-ideal mixing, the actual configurational contribution to the Gibb's free energy will be less. At the synthesis temperature of 1300 °C and applying the ideal mixing assumption, the ideal configurational entropic contribution to Gibb's free energy ( $-T\Delta S_{mix}$ ) is calculated to be  $-11.2$  kJ/mol. By comparing the ideal configurational entropy and the enthalpy of mixing as recorded by calorimetry, enthalpic effects and entropic effects provide comparable contributions to the stability of mixed HfTiO<sub>4</sub>-ZrTiO<sub>4</sub> compounds. The result is that enthalpic effects are insufficient to cause changes in bulk symmetry upon mixing in the (Hf-Zr)TiO<sub>4</sub> system.

Positive  $\Delta H_{f,ox}$  values for HfTiO<sub>4</sub> and ZrTiO<sub>4</sub> suggest that Hf-Ti and Zr-Ti local segregation is possible. Positive  $\Delta H_{f,ox}$  values for mixed HfTiO<sub>4</sub>-ZrTiO<sub>4</sub> compounds shows that the (Hf-Zr)TiO<sub>4</sub> system is entropy stabilized with respect to the constituent oxides. Upon mixing HfTiO<sub>4</sub> and ZrTiO<sub>4</sub>, a negative  $\Delta H_{mix}$  was observed. This negative  $\Delta H_{mix}$  demonstrates that mixing between HfTiO<sub>4</sub> and ZrTiO<sub>4</sub> is non-ideal and implies that secondary ordering between Hf and Zr could be occurring. To

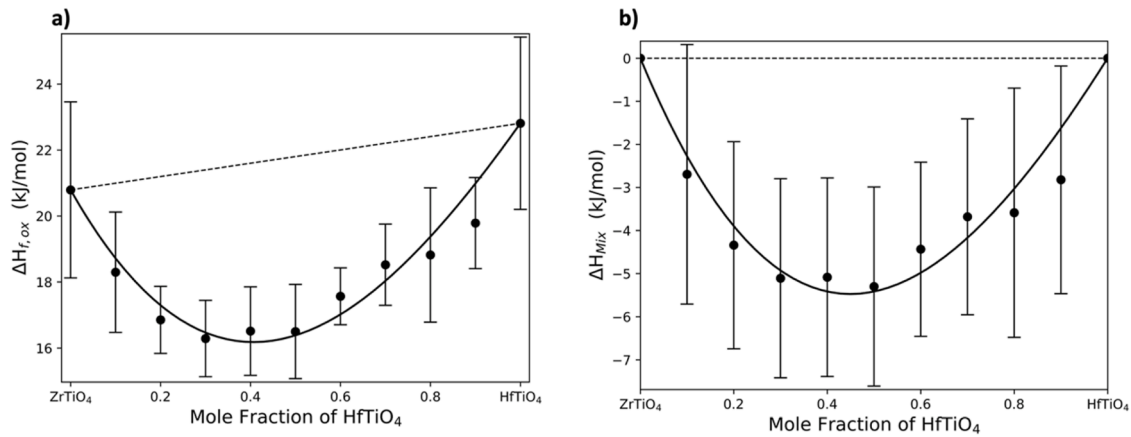


**Fig. 2.** (a) Formation enthalpy relative to the constituent oxides ( $x_1\text{ZrTiO}_4$  and  $x_2\text{HfTiO}_4$ ) in comparison to the  $(\text{Zr}_{x_1},\text{Hf}_{x_2})\text{TiO}_4$  mixed compound. The dashed black line shows the ideal mixing (i.e. excess enthalpy is zero) enthalpy across the system. (b) Enthalpy of mixing ( $\Delta H_{\text{mix}}$ ) in the  $(\text{Zr}_{x_1},\text{Hf}_{x_2})\text{TiO}_4$  system. Measurement uncertainty is denoted by error bars. Data was fit to the Sub-Regular Solution model. Fit statistics for the Sub-Regular solution model are as follows:  $A = -17.162$  kJ/mol,  $B = -26.171$  kJ/mol,  $R^2 = 0.9205$ . Data relevant to Fig. 2 can be found in the S5, S6.

**Table 2**

Enthalpy of formation from constituent oxides and constituent elements for  $\text{HfTiO}_4$  and  $\text{ZrTiO}_4$  as determined by this study, and as determined by Hom et al. [57]. Values for  $\text{HfTiO}_4$  were not reported by Hom. Measurement uncertainty (MU) is defined as two times the standard error ( $\frac{2\sigma}{\sqrt{N}}$  where  $\sigma$  is the standard deviation and  $N$  is the number of measurements).

Compound	$\Delta H_{f,ox}$ (kJ/mol) (mean $\pm$ MU)	$\Delta H_{f,el}$ (kJ/mol)
$\text{HfTiO}_4$ (This study)	$22.81 \pm 2.61$	-2033.510
$\text{ZrTiO}_4$ (This study)	$20.79 \pm 2.67$	-2015.39
$\text{ZrTiO}_4$ (Hom et. al)	20.23	-2024.4

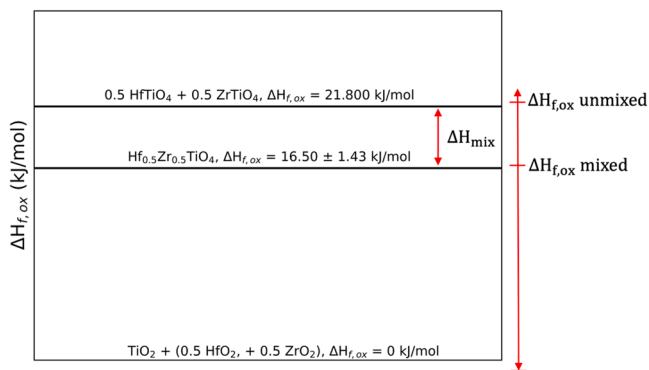


**Fig. 3.** Vertical enthalpy diagram for  $(\text{Hf}_{0.5},\text{Zr}_{0.5})\text{TiO}_4$ . The y-axis is enthalpy of formation relative to the constituent oxides. The top line shows the enthalpy of the ideally mixed mixture of  $0.5\text{HfTiO}_4$  and  $0.5\text{ZrTiO}_4$  ( $\Delta H_{f,ox}^{\text{unmixed}}$ ), the middle line shows the enthalpy of the system when  $\text{HfTiO}_4$  and  $\text{ZrTiO}_4$  form a single-phase product ( $(\text{Hf}_{0.5},\text{Zr}_{0.5})\text{TiO}_4$ ) ( $\Delta H_{f,ox}^{\text{mixed}}$ ), and the bottom line is the enthalpy of the constituent oxides (reference point). The lower the line on the plot, the more enthalpically stable.

probe the length scales at which this ordering occurs in the system, and to assess their impacts on lattice parameters, XRPD was performed on the  $(\text{Hf-Zr})\text{TiO}_4$  system.

### 3.2. Excess volume

XRPD data shows that all members of the  $(\text{Hf-Zr})\text{TiO}_4$  system form single-phase non-ideal solid solution with Pbcn symmetry. This result indicates that mixing does not change the long-range structure of the

system. This is evidenced by the lack of satellite peaks corresponding to superstructures in the XRPD data. It must be noted that while XRPD shows that the  $(\text{Hf-Zr})\text{TiO}_4$  system forms a non-ideal single-phase solid solution when examined at larger length scales, XRPD is unable to probe the local structure of the system. Thus, local structure non-idealities in the  $(\text{Hf-Zr})\text{TiO}_4$  system are studied using XAS as discussed in Section 3.3.

Fig. 4 shows a waterfall plot of the  $(\text{Hf-Zr})\text{TiO}_4$  system as function of  $\text{HfTiO}_4$  mol fraction. The first key observation is that  $(\text{Hf-Zr})\text{TiO}_4$  forms a single phase across the entire composition range, as noted by each peak being indexed to the Pbcn structure shown in Fig. 1. The peaks corresponding to the (200), (020), and (002) indices are principal components and are directly related to the magnitude of the a, b and c lattice vectors respectively. On inspection, the (020) (b-lattice vector) is expanding, as noted by the shift to the left, the (200) (a-lattice vector) is contracting, as noted by the shift to the right and the (020) (c-lattice vector) is relatively constant. These observations show that the lattice volume expansion of the unit cell is highly anisotropic. The volume and lattice parameters for the  $(\text{Hf-Zr})\text{TiO}_4$  system were extracted by applying the Rietveld method [70] to XRPD and are plotted in Fig. 5(a) and Fig. 6 (a) respectively. To understand how non-ideal mixing in the  $(\text{Hf-Zr})\text{TiO}_4$  system effects volume, the excess volume for  $(\text{Hf-Zr})\text{TiO}_4$  system was determined by subtracting the measured volume of mid points in the  $(\text{Hf-Zr})\text{TiO}_4$  system from an ideal mixture of volumes (Eqs. (11), (12)).

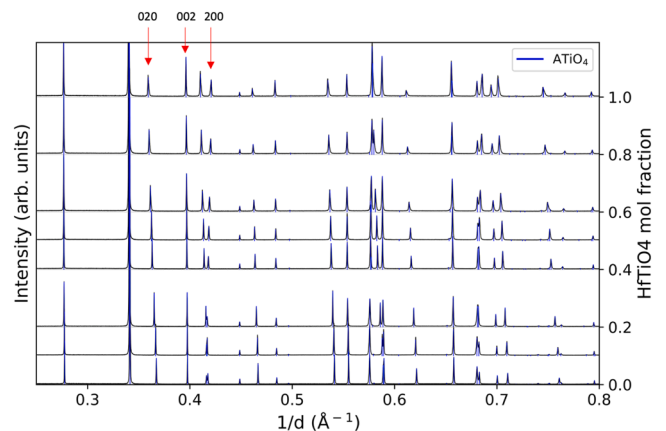


**Fig. 4.** Waterfall plot of Synchrotron 11-BM XRPD data across the  $(\text{Hf-Zr})\text{TiO}_4$  system. Blue lines are peak positions determined from Rietveld Refinement. Powder diffraction peaks corresponding to the lattice vectors of the unit cell are denoted with red arrows. Data relevant to Fig. 4 can be found in the Supplementary Information S1, S2, and S7.

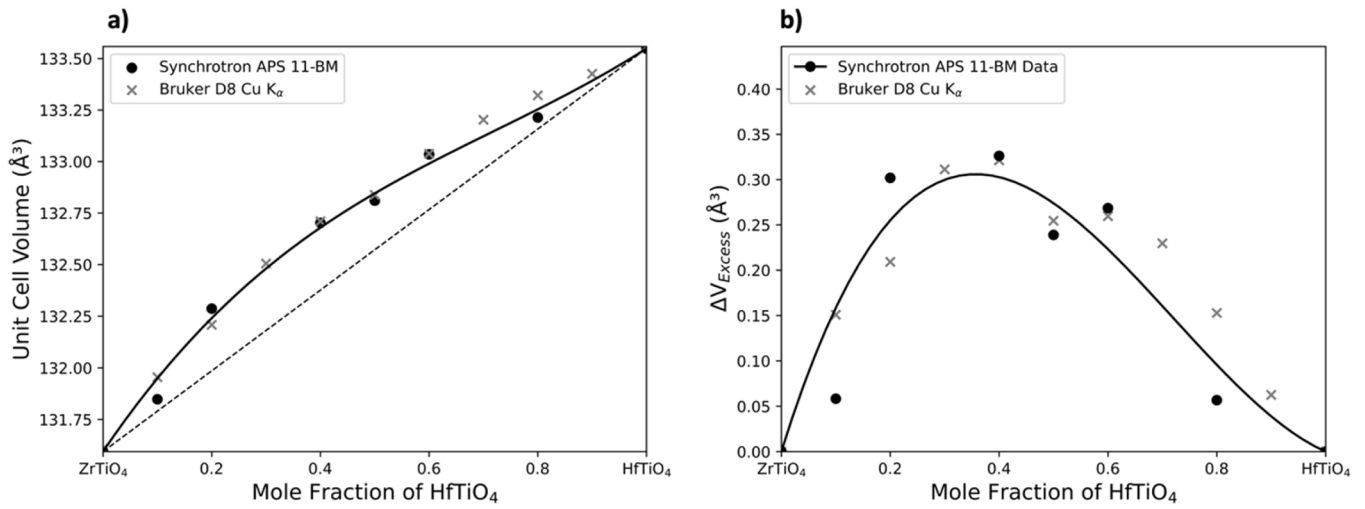


**Fig. 5.** Shows that there is a positive excess volume in the (Hf-Zr)TiO<sub>4</sub> system. As with mixing enthalpy, the distribution peak skews off-center in the direction of the Zirconium rich compounds. The (Hf-Zr)TiO<sub>4</sub> system was determined to have maximum excess volume of  $\Delta V_{\text{mix}} = .3260 \text{ \AA}^3$  at a composition of (Hf<sub>4</sub>Zr<sub>0.6</sub>)TiO<sub>4</sub>. The excess volume for the system is positive (0.18 % increase), indicating that mixing HfTiO<sub>4</sub> and ZrTiO<sub>4</sub> is non-ideal and leads substantial strain on the crystal lattice. Data relevant to Fig. 5 can be found in the Supplementary Information S1, S2 and S7.

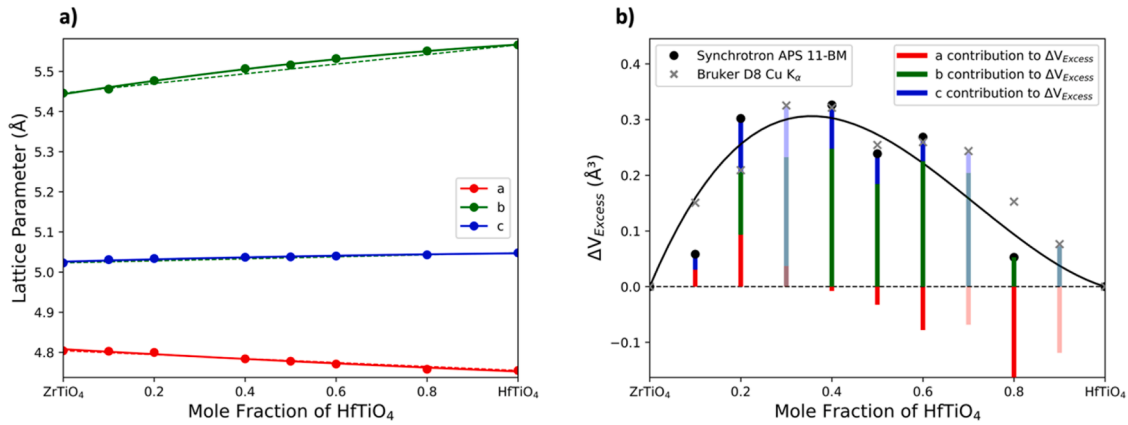


**Fig. 6.** (a) Lattice parameters vs composition for the (Hf-Zr)TiO<sub>4</sub> system. Lattice parameters were determined through Rietveld Refinement of Synchrotron data recorded at the APS 11-BM beamline. Lattice parameters for  $x_{\text{HfTiO}_4} = 0.3, 0.7, 0.9$  are not shown as they were not measured at the APS 11-BM beamline. Lattice parameters were fit using 2nd order polynomials. The dashed lines indicate the ideal lattice parameter (linear combination) across all compositions. (b) Contribution of each lattice parameter to the excess volume in the (Hf-Zr)TiO<sub>4</sub> system. Excess volume is the same in Fig. 5(b). Lab source data for  $\Delta V_{\text{excess}}$  and lattice parameters were used to fill in points where Synchrotron data was unavailable. Parameter contribution for lab source data is shown as faded bars. Lattice parameter fits and values at each composition are reported in the supplementary information. Data relevant to Fig. 2 can be found in the Supplementary Information S1, S2 and S7.

$$\Delta V_{\text{idealmixing}}^{x_1 \text{HfTiO}_4 + x_2 \text{ZrTiO}_4} = x_1 \Delta V_{\text{measured}}^{\text{HfTiO}_4} + x_2 \Delta V_{\text{measured}}^{\text{ZrTiO}_4} \quad (11)$$

**Eq. (11):** Ideal mixing volumes for the (Hf-Zr)TiO<sub>4</sub> system (i.e. the excess volume is zero).  $x_1$  is the mole fraction of HfTiO<sub>4</sub> and  $x_2$  is the mole fraction of ZrTiO<sub>4</sub>.  $\Delta V_{\text{measured}}^{\text{HfTiO}_4}$  and  $\Delta V_{\text{measured}}^{\text{ZrTiO}_4}$  are the volumes of the endpoints as determined by Rietveld Refinement.

$$\Delta V_{\text{excess}}^{(\text{Hf}_{x_1} \text{Zr}_{x_2})\text{TiO}_4} = \Delta V_{\text{measured}}^{(\text{Hf}_{x_1} \text{Zr}_{x_2})\text{TiO}_4} - \Delta V_{\text{idealmixing}}^{x_1 \text{HfTiO}_4 + x_2 \text{ZrTiO}_4} \quad (12)$$

**Eq. (12):** Calculation of Excess volume for any composition in the (Hf-Zr)TiO<sub>4</sub> system.  $x_1$  is the mole fraction of HfTiO<sub>4</sub> and  $x_2$  is the mole fraction of ZrTiO<sub>4</sub>.  $\Delta V_{\text{measured}}^{(\text{Hf}_{x_1} \text{Zr}_{x_2})\text{TiO}_4}$  and  $\Delta V_{\text{measured}}^{x_1 \text{HfTiO}_4 + x_2 \text{ZrTiO}_4}$  are the volumes of the endpoints as determined by Rietveld Refinement.

Excess volume was also fit to the sub-regular solution model as it provided the best fit (Eq. (13)).

$$\Delta V_{\text{excess}} = A_v x_1^2 x_2 + B_v x_1 x_2^2 \quad (13)$$

**Eq. (13):** Sub regular solution model for excess volume.  $A_v$  and  $B_v$  are the volume-specific fit parameters,  $x_1$  is the mole fraction of HfTiO<sub>4</sub> and

$x_2$  is the mole fraction of ZrTiO<sub>4</sub>. Fit parameters and statistics are shown in S7 of supplemental information.

The overall volume expansion is anisotropic with a positive contribution in the b-direction, a negative contribution in the a-direction and negligible contribution in the c-direction. Thus, the excess lattice parameter ( $\Delta a_{\text{excess}}$ ) in the (Hf-Zr)TiO<sub>4</sub> system was determined by subtracting the ideal mixing lattice parameters ( $\Delta a_{\text{ideal}}$ , Eq. (14)) from the lattice parameters determined through Rietveld Refinement of XRPD data (Eq. (15)).

$$\Delta a_{\text{idealmixing}}^{x_1 \text{HfTiO}_4 + x_2 \text{ZrTiO}_4} = x_1 \Delta a_{\text{measured}}^{\text{HfTiO}_4} + x_2 \Delta a_{\text{measured}}^{\text{ZrTiO}_4} \quad (14)$$

**Eq. (14):** Linear combination of lattice parameters ( $\Delta a_{\text{ideal}}$ ) calculated from the lattice parameters of the experimental endpoints ( $\Delta a_{\text{measured}}^{\text{HfTiO}_4}$ ,  $\Delta a_{\text{measured}}^{\text{ZrTiO}_4}$ ) in the (Hf-Zr)TiO<sub>4</sub> system.  $x_1$  is the mole fraction of HfTiO<sub>4</sub> and  $x_2$  is the mole fraction of ZrTiO<sub>4</sub>.

$$\Delta a_{\text{excess}}^{(\text{Hf}_{x_1} \text{Zr}_{x_2})\text{TiO}_4} = \Delta a_{\text{measured}}^{(\text{Hf}_{x_1} \text{Zr}_{x_2})\text{TiO}_4} - \Delta a_{\text{idealmixing}}^{x_1 \text{HfTiO}_4 + x_2 \text{ZrTiO}_4} \quad (15)$$

Eq. (15): Calculation of excess lattice parameter ( $\Delta a_{\text{excess}}$ ) from measured lattice parameters ( $\Delta a_{\text{measured}}^{(\text{Hf}_{x_1}, \text{Zr}_{x_2})\text{TiO}_4}$ ) and ideal lattice parameters ( $\Delta a_{\text{idealmixing}}^{x_1\text{HfTiO}_4+x_2\text{ZrTiO}_4}$ ) for any composition in the (Hf-Zr)TiO<sub>4</sub> system.

Excess lattice parameters were calculated at each composition and divided by the summation of all excess lattice parameters at that composition to determine the percent contribution from the excess. The resulting values were multiplied by excess volume to determine the percent contribution of each lattice parameter to excess volume. Eq. (16) shows the calculation for excess lattice parameter contribution at any specified composition.

$$\Delta a_{\text{contribution}}^i = \Delta V_{\text{excess}} \left( \frac{a_i^{\text{excess}}}{\sum_{i=1}^3 a_i^{\text{excess}}} \right) \quad (16)$$

Eq. (16): Calculation of lattice parameter contribution to excess volume.  $a_{1,2,3} = a, b, c$  parameters respectively.

Fig. 6b shows the contribution of each lattice parameter to the measured excess volume in the (Hf-Zr)TiO<sub>4</sub> system. This shows that the excess contribution of the b-lattice vector is dominating the overall excess volume expansion in the (Hf-Zr)TiO<sub>4</sub> system. As mentioned in Section 1.2, in ZrTiO<sub>4</sub> samples, the b-lattice parameter is cooling rate dependent. As cooling rate is increased, the b-parameter grows larger. The b-lattice parameter dependence on cooling rate is similar to the observed b-lattice parameter change in mixed (Hf-Zr)TiO<sub>4</sub> samples. All (Hf-Zr)TiO<sub>4</sub> samples were synthesized with a consistent cooling rate of 5C/min. Thus, changes in b-lattice parameter are attributed solely to changes in composition.

XRPD and subsequent Rietveld refinement shows that there is a positive anisotropic excess volume for the (Hf-Zr)TiO<sub>4</sub> system. This

result further proves that mixing in the system is not ideal. XRPD patterns do not show the presence of superlattice peaks, indicating that the observed excess volume and enthalpy are a result of non-ideal mixing on the local scale. To validate this assertion, the local structure of the (Hf-Zr)TiO<sub>4</sub> system was studied using X-ray absorption spectroscopy (XAS).

### 3.3. X-ray absorption spectroscopy and local structure

XAS, specifically in the X-ray absorption near edge structure (XANES) and extended X-ray absorption fine structure (EXAFS), is documented as useful tool for studying local environments in mixed chemical systems [79,80]. To study the local environment and to provide insight on non-ideal mixing in the (Hf-Zr)TiO<sub>4</sub> system, XAS was performed. Fig. 7(a) presents the XANES spectrum for the Ti K-edge for all samples across the composition range. There is little variation in these spectra, indicating that the Ti local environment is constant throughout the composition range. Fig. 7(d) shows the Ti EXAFS fit for (Hf<sub>5</sub>Zr<sub>5</sub>)TiO<sub>4</sub> and is typical of all the Ti edge EXAFS which can be fitted using a model with 2 Ti-O paths (1.9 Å and 2.0 Å) with multiplicities 4 and 2 and a Ti-Ti path (2.8 Å) with multiplicity ~2-3. There is no evidence of any Ti-Zr or Ti-Hf scattering paths in any of the Ti edge data (SI section S8).

The XANES spectra for Zr and Hf (Fig. 7 (b,c)) exhibit isosbestic points, indicating that the Zr and Hf atoms reside in two distinct local environments; local environment 1 being a local structure of 100 % Zr (Hf) next near neighbors and local environment 2 being dilute Zr (Hf) in a second near neighbor environment of mostly Hf (Zr). Furthermore, consistent with the Ti K-edge EXAFS, the Zr and Hf EXAFS in ZrTiO<sub>4</sub> and HfTiO<sub>4</sub>, respectively can be fit without Zr-Ti and Hf-Ti paths as shown in

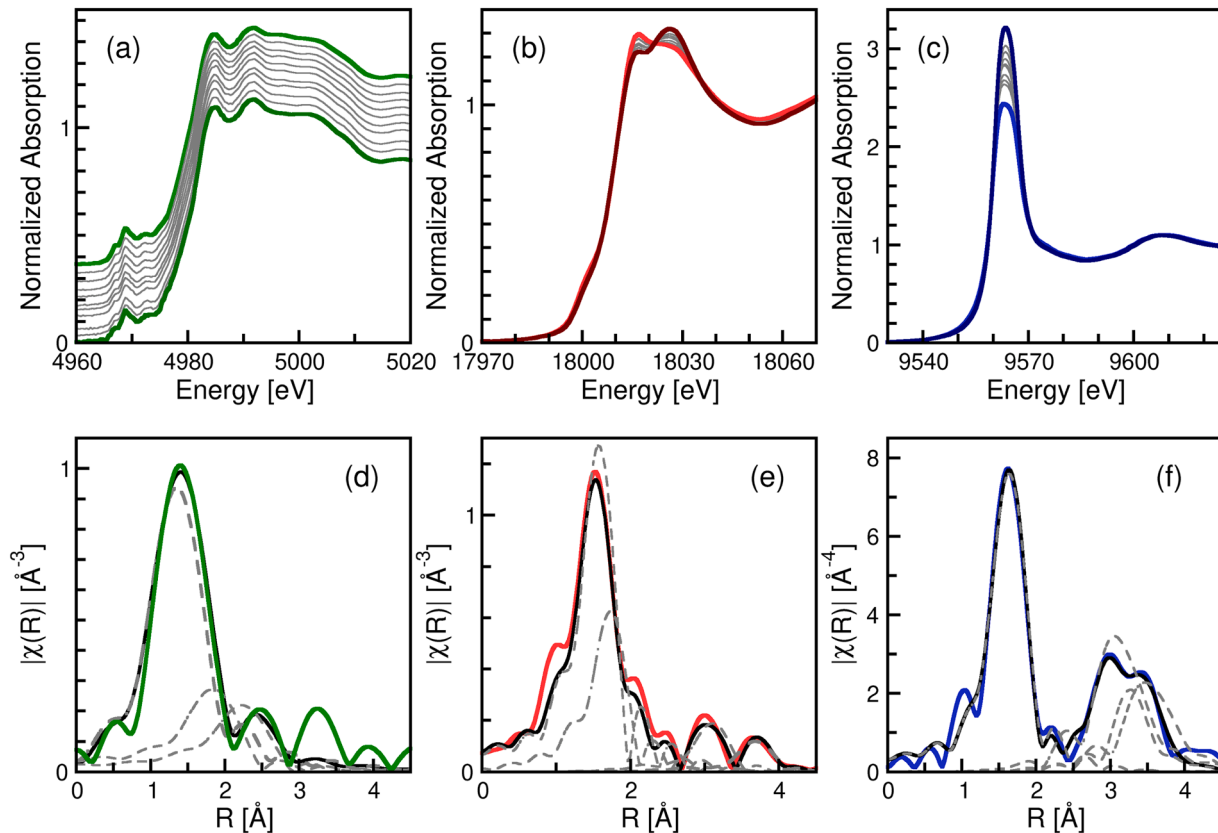


Fig. 7. (a) XANES spectra for the Ti K-edge of the (Zr<sub>1-x</sub>Hf<sub>x</sub>)TiO<sub>4</sub> system with HfTiO<sub>4</sub> at the bottom and ZrTiO<sub>4</sub> at the top; (b) Zr K-edge XANES for ZrTiO<sub>4</sub> (light red) through (Zr<sub>0.1</sub>Hf<sub>0.9</sub>)TiO<sub>4</sub> (dark red); (c) Hf L<sub>3</sub>-edge XANES for HfTiO<sub>4</sub> (light blue) through (Zr<sub>0.9</sub>Hf<sub>0.1</sub>)TiO<sub>4</sub> (dark blue); (d) Ti K-edge EXAFS spectrum (green) and fit (black) for the (Zr<sub>0.5</sub>Hf<sub>0.5</sub>)TiO<sub>4</sub> sample showing the individual paths making up the fit (grey dashed); (e) Zr K-edge EXAFS spectrum (red) and fit (black) for the ZrTiO<sub>4</sub> sample showing the individual paths making up the fit (grey dashed); (f) Hf L<sub>3</sub>-edge EXAFS spectrum (blue) and fit (black) for the HfTiO<sub>4</sub> sample showing the individual paths making up the fit (grey dashed).

Fig. 7 (e,f). The Zr local environment consists of 2 Zr-O paths (2.06 Å and 2.22 Å) with multiplicities of  $\sim 4$  and  $\sim 2$  and two Zr-Zr paths (3.47 Å and 4.08 Å) with multiplicities  $\sim 2$  each. The Hf local environment, in contrast, shows a single Hf-O path (2.05 Å) with multiplicity  $\sim 6$ , two Hf-Hf paths (3.27 Å and 3.68 Å) with multiplicities of  $\sim 4$  each and a second Hf-O path (3.73 Å) with multiplicity of 4. These results indicate that Ti, Zr, and Hf all preferentially reside in local environments made up of identical species rather than mixing uniformly spatially. To test this hypothesis, the Zr and Hf XANES and EXAFS data for all samples were fitted using the endpoint samples data,  $\text{ZrTiO}_4$  and  $(\text{Zr}_{0.1}\text{Hf}_{0.9})\text{TiO}_4$  for the Zr edge,  $\text{HfTiO}_4$  and  $(\text{Zr}_{0.1}\text{Hf}_{0.9})\text{TiO}_4$  for the Hf edge. The results of the fits for the XANES spectra are shown in Fig. 8, where the fraction of the pure  $\text{HfTiO}_4$  and  $\text{ZrTiO}_4$  endpoints used to fit the individual spectra are plotted as a function of the nominal sample composition. The Zr edge data, which have a distinct variation across the composition range, exhibit a nearly straight diagonal line while the Hf data, which have more subtle differences show a similar diagonal trend albeit with a lower slope.

### 3.4. Discussion of non-ideal mixing in the (Hf-Zr)TiO<sub>4</sub> system

Transmission electron microscopy (TEM) studies on  $\text{ZrTiO}_4$  have shown that the compound is not perfectly disordered as is indicated by bulk X-ray powder diffraction, and that Zr and Ti segregate locally [43–52].  $\text{ZrTiO}_4$  additionally has low temperature ordered modulated superstructures that have been reported to form exceptionally slowly below  $\sim 1147$  °C. The ordered structures occupy a composition range that spans from  $\text{ZrTiO}_4$  to compositions close to  $\text{ZrTi}_2\text{O}_6$ .  $\text{Zr}_5\text{Ti}_7\text{O}_{24}$  is the most frequently observed and studied low temperature ordered phase in the system. Using TEM and single crystal diffraction, Christoffersen and Davies [47] showed that compositions of  $\text{Zr}/\text{Ti} = 5/7$  and  $1/1$  have incommensurate superstructures, and phases close to  $1/1$  are commensurate with an a-axis repeat of  $2x$  compared to the long-range disordered  $\text{ZrTiO}_4$  structure. This commensurate/incommensurate transition is marked by Zr segregation onto every 3rd octahedra site on a

given axis, leading to the formation of the triple celled  $\text{Zr}_5\text{Ti}_7\text{O}_{24}$  super structure. This ordering can be as represented as  $\text{Z}^{\text{TT}}\text{Z}_{\text{TT}}$ , where  $\text{Z}^{\text{TT}}$  denotes a Zr octahedra neighboring a pair of Ti octahedra aligned upwards, and  $\text{Z}_{\text{TT}}$  denotes a Zr octahedra neighboring a pair of Ti octahedra aligned downwards. Results showed that the  $\text{Z}^{\text{TT}}\text{Z}_{\text{TT}}$  repeating sequence is sporadically broken up by double layers of Zr, with the sequence  $\text{ZZ}^{\text{TT}}$  (or  $\text{ZZ}_{\text{TT}}$ ), giving rise to an additional  $\text{Z}^{\text{TT}}\text{ZZ}_{\text{TT}}$  motif in the low temperature ordered  $\text{Zr}_5\text{Ti}_7\text{O}_{24}$  phase [49]. Additionally, electron diffraction patterns showed the presence of superlattice formation in  $\text{Zr}_5\text{Ti}_7\text{O}_{24}$  samples [47–49]. Smaller more diffuse superlattice peaks were also observed in electron diffraction for commensurate  $\text{ZrTiO}_4$ , indicating that some additional long-range ordering may be present. Unfortunately, peaks intensities were too weak for any structural refinement. TEM analysis showed no substantial difference between quenched and slow-cooled samples [47–49].

In samples that show the long-range disordered  $\text{ZrTiO}_4$  structure, the  $\text{ZZ}^{\text{TT}}$  sequence dominated on the local level. In these samples, TEM bright field analysis performed by Azough et al. [49] confirmed the presence of the  $\text{ZZ}^{\text{TT}}\text{ZZ}_{\text{TT}}$  and  $\text{Z}^{\text{TT}}\text{Z}_{\text{TT}}$  motif. Christoffersen and Davies [47] argue that due to the differing preferred oxygen coordination of Zr (4 Zr-O bonds, cubic) and Ti (6 Ti-O bonds, octahedra), that the two cations prefer not to be neighbors, leading to local cation segregation. This segregation of Zr and Ti is stated to influence the b-lattice parameter of the bulk disordered  $\text{ZrTiO}_4$  structure. Lopez-Lopez et al. and Azough et al. [48,49] both have studied the effect cooling rate has on lattice parameters in  $\text{ZrTiO}_4$  compounds. X-ray diffraction experiments show that altering cooling rate leads to a marked shift in peak position. Faster cooling rate led to larger b-lattice parameters, as well as larger crystal lattice volume. Lopez-Lopez reported b-lattice parameters of 5.47731 Å in quenched samples, 5.4389 Å in samples cooled at 5 °C /min, and 5.4174 Å in samples cooled at 0.1 °C /min. Similar values were reported by Azough et al. Cooling rate dependent changes in the b-lattice parameter are attributed to the presence of ordering in the system. Quenching samples locks in the disordered high-temperature state where the  $\text{ZZ}^{\text{TT}}\text{ZZ}_{\text{TT}}$  and  $\text{Z}^{\text{TT}}\text{Z}_{\text{TT}}$  motifs do not occur at a local level, thus eliminating distortions in the b-direction.

XAS results in this work are consistent with literature data on local structure in  $\text{ZrTiO}_4$ . Both techniques agree that Zr and Ti are segregating locally in a ratio that randomizes over the bulk and maintains the disordered structure as observed in XRPD.  $\text{HfTiO}_4$  experiences similar local segregation between Hf and Ti. Cation segregation was also observed in mixed  $\text{HfTiO}_4$ - $\text{ZrTiO}_4$  samples, resulting in the separate clusters of Hf/Zr and Ti.

XAS results in mixed  $\text{HfTiO}_4$ - $\text{ZrTiO}_4$  samples shows that Hf/Zr clusters are not mixed ideally. Within the Hf/Zr clusters, Hf and Zr cations can exist in two possible local environments; an Hf or Zr cation surrounded exclusively by one of Hf or Zr. Unfortunately, the exact ratio of cations in each unique environment, as well as the spatial orientation of the clusters, cannot be determined quantitatively from XAS. It is hypothesized that short-range ordering (SRO) of Hf and Zr in mixed (Hf-Zr) TiO<sub>4</sub> samples occurs on similar length scales to the Zr-Ti segregation observed by Christoffersen and Davies [47], but further experimentation is needed to confirm. Clusters are randomized at longer length scales, as noted by bulk XRPD data showing no signs of phase separation or satellite peaks in the synchrotron powder diffraction patterns. To fully understand non-ideal mixing at the local level in (Hf-Zr)TiO<sub>4</sub> system, high resolution TEM experiments are needed. XAS data can be used to conclude that Hf/Zr segregate from Ti to form local clusters, and that mixing within the Hf/Zr cluster is non-ideal. The result is that the (Hf-Zr) TiO<sub>4</sub> system is not truly disordered, even though  $\text{HfTiO}_4$  and  $\text{ZrTiO}_4$  are entropy stabilized with respect to the constituent oxides.

Hf and Zr intermingling can be further rationalized by looking at bond lengths. Both atoms prefer to exist with octahedral oxygen coordination, which is why Hf and Zr octahedra can intermingle further. EXAFS analysis on nearest neighbor pairs provided cation-oxygen bond lengths for the (Hf-Zr)TiO<sub>4</sub> system. In all samples, Ti octahedra

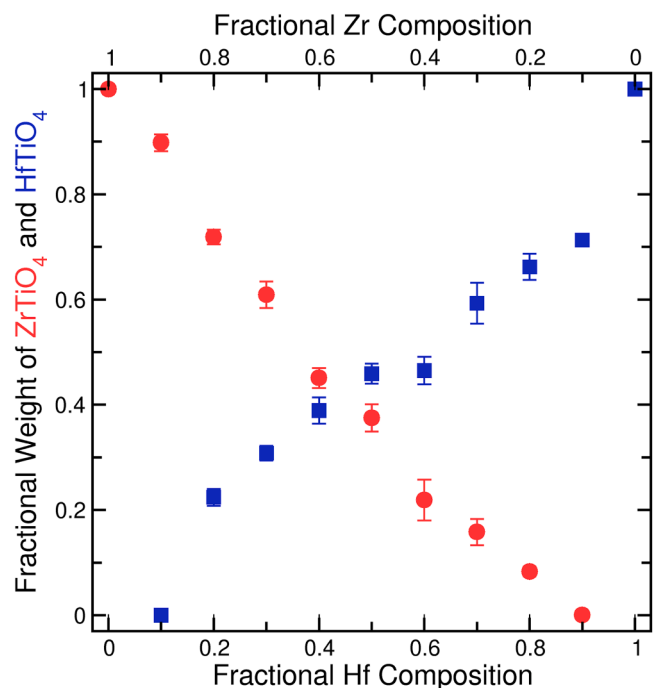


Fig. 8. Fractional weight of  $\text{ZrTiO}_4$  (red circles) and  $\text{HfTiO}_4$  (blue squares) obtained from single parameter fits of the Zr and Hf XANES spectra with the endpoint compositions (100 % and 10 % Zr and Hf). Individual fits are shown in SI section S8.

experienced a Jahn-Teller elongation, with an equatorial bond length of 2.00 Å and an axial bond length 2.43 Å. Zr octahedra also experience a Jahn-Teller elongation; Zr-O bond lengths were determined to be 2.06 Å in the equatorial direction and 2.22 Å in the axial direction. In the case of Hf-O, only a bond length of 2.06 Å was found, meaning that Hf octahedra do not experience distortion. Due to differing axial lengths, it is reasonable that Hf and Zr octahedra would prefer to exist independently of one another, giving rise to the secondary clustering within the Hf/Zr cation layer.

Christofferson and Davies [47] noted that cluster size in cation layers depends on directionality. These cluster switches occurred at different rates in different directions in the crystal lattice, with cation cluster sizes ranging from 5 to 20 nm in the b-direction and 50 nm in the c-direction. It is possible that directionally preferential arrangement of Jahn-Teller elongated Zr-O polyhedra and non-distorted Hf-O polyhedra could generate the observed anisotropic excess volume within the (Hf-Zr)TiO<sub>4</sub> system. Altering the Zr concentration in the (Hf-Zr)TiO<sub>4</sub> system would lead to changes in Zr sub-cluster size and frequency, causing anisotropic distortions to the average bulk volume. Again, these local clusters are randomizing in terms of composition but are maintaining a directionality. This is noted by the excess change in b-lattice parameter and the lack of superlattice peaks in the X-ray powder diffraction pattern. As before, to fully elucidate the mechanisms of polyhedra stacking, further experiments like high resolution TEM are needed.

Local structural findings from XAS agrees with calorimetry data. Both HfTiO<sub>4</sub> and ZrTiO<sub>4</sub> have a positive enthalpy of formation relative to the constituent oxides (HfO<sub>2</sub>, ZrO<sub>2</sub>, TiO<sub>2</sub>), suggesting that Hf-Ti and Zr-Ti do not prefer to mix. XAS showed that in both HfTiO<sub>4</sub> and ZrTiO<sub>4</sub> there is distinct Hf-Ti and Zr-Ti local segregation. In mixed (Hf-Zr)TiO<sub>4</sub> samples, the negative mixing enthalpy relative to HfTiO<sub>4</sub> and ZrTiO<sub>4</sub> endpoints implies that Hf and Zr cations experience non-ideal mixing. XAS results confirm that mixing between Hf and Zr is non-ideal, but that the two cations intermingle and form separate clusters from Ti. To gain insight into potential ordering between Hf and Zr, further experimentation is needed.

Synthesis routes have been demonstrated to have a marked effect on structural and chemical features such as grain morphology, oxygen stoichiometry, local distortions, and chemical homogeneity in the HEO spinel structure [81]. Despite local variations, the average structure, as determined by XRPD, for the HEO spinel was consistent across different synthetic routes and resembles that of the thermodynamically favorable product. Thus, it can be assumed that (Hf-Zr)TiO<sub>4</sub> prepared through steric entrapment could have slightly different local features when compared to a (Hf-Zr)TiO<sub>4</sub> sample prepared through a different method, all while maintaining the observed X-ray diffraction pattern.

#### 4. Conclusions

In this study, 11 compositions in the entropy stabilized (Hf-Zr)TiO<sub>4</sub> system were synthesized. It was determined through oxide melt calorimetry that there is a negative enthalpy of mixing within the system with respect to HfTiO<sub>4</sub> and ZrTiO<sub>4</sub>. This implies that mixing in the system is enthalpically preferred with respect to ZrTiO<sub>4</sub> and HfTiO<sub>4</sub>, highlighting non-ideal mixing. It needs to be made clear that (Hf-Zr)TiO<sub>4</sub> compounds are entropy stabilized with respect to the component oxides (TiO<sub>2</sub>, ZrO<sub>2</sub> and HfO<sub>2</sub>). The negative enthalpy of mixing is contrasted by the determination of a positive excess volume. Additionally, the excess volume is highly anisotropic, with the majority of contributions to excess volume resulting from change in the b lattice parameter. XAS data from this study was used to confirm that mixing in the HfTiO<sub>4</sub>-ZrTiO<sub>4</sub> system is non-ideal and that cations segregate locally to form independent clusters of Hf/Zr and Ti. In mixed HfTiO<sub>4</sub>-ZrTiO<sub>4</sub> samples, it was determined that there are two local environments within the Hf/Zr cluster, indicating that mixing between Hf and Zr is also non-ideal. Results from XAS were used in conjunction with a past TEM study on ZrTiO<sub>4</sub> to build a hypothesis on the source of the negative mixing

enthalpy and positive excess volume observed in the (Hf-Zr)TiO<sub>4</sub> system. TEM is still needed to fully elucidate the local structure and potential SRO within the Hf/Zr cluster. Using the (Hf-Zr)TiO<sub>4</sub> system as a case study, this work demonstrates that mixing in entropy stabilized oxides is not always ideal, and that enthalpic contributions can lead to the formation of complex local structures that effect the physical and chemical properties of a system.

#### CRedit authorship contribution statement

**William Rosenberg:** Writing – review & editing, Writing – original draft, Methodology, Formal analysis, Data curation. **Stuart C. Ness:** Writing – review & editing, Writing – original draft, Methodology, Data curation. **Bhoopesh Mishra:** Writing – review & editing, Writing – original draft, Formal analysis, Data curation. **Carlo U. Segre:** Writing – review & editing, Writing – original draft, Formal analysis, Data curation. **Scott J. McCormack:** Writing – review & editing, Supervision, Project administration, Conceptualization.

#### Declaration of competing interest

The authors declare that they have no known competing financial interests or personal relationships that could have appeared to influence the work reported in this paper.

#### Acknowledgements

This work was funded by the National Science Foundation (NSF) in the Directorate for Mathematical and Physical Sciences (MPS), under the Division of Materials Research (DMR), in the Ceramic (CER) program. Award number: 2047084. MRCAT operations are supported by the Department of Energy and the MRCAT member institutions. This research used resources of the Advanced Photon Source, a U.S. Department of Energy (DOE) Office of Science User Facility operated for the DOE Office of Science by Argonne National Laboratory under Contract No. DE-AC02-06CH11357.

#### Supplementary materials

Supplementary material associated with this article can be found, in the online version, at [doi:10.1016/j.actamat.2024.120639](https://doi.org/10.1016/j.actamat.2024.120639).

#### References

- [1] J.W. Yeh, S.K. Chen, S.J. Lin, J.Y. Gan, T.S. Chin, T.T. Shun, C.H. Tsau, S.Y. Chang, Nanostructured high-entropy alloys with multiple principal elements: novel alloy design concepts and outcomes, *Adv. Eng. Mater.* 6 (5) (2004) 299–303, <https://doi.org/10.1002/ADEM.200300567>.
- [2] Guo, S., & Liu, C.T. (2011). Phase stability in high entropy alloys: formation of solid-solution phase or amorphous phase.
- [3] D.B. Miracle, High entropy alloys as a bold step forward in alloy development, *Nat. Commun.* 10 (1) (2019) 1–3, <https://doi.org/10.1038/s41467-019-09700-1>. 2019 10:1.
- [4] S. Gorsse, J.P. Couzinié, D.B. Miracle, From high-entropy alloys to complex concentrated alloys, *Comptes Rendus Physique* 19 (8) (2018) 721–736, <https://doi.org/10.1016/j.crchy.2018.09.004>.
- [5] Oses, C., Toher, C., & Curtarolo, S. (2020). High-entropy ceramics. [10.1038/s41578-019-0170-8](https://doi.org/10.1038/s41578-019-0170-8).
- [6] R. Djenadic, A. Sarkar, O. Clemens, C. Loho, M. Botros, V.S.K. Chakravadhanula, C. Kübel, S.S. Bhattacharya, A.S. Gandhi, H. Hahn, Multicomponent Eq. uiatomic rare earth oxides, *Mater. Res. Lett.* 5 (2) (2017) 102–109, <https://doi.org/10.1080/21663831.2016.1220433>.
- [7] A. Sarkar, Q. Wang, A. Schiele, M.R. Chellali, S.S. Bhattacharya, D. Wang, T. Brezesinski, H. Hahn, L. Velasco, B. Breitung, High-entropy oxides: fundamental aspects and electrochemical properties, *Adv. Mater.* 31 (26) (2019), <https://doi.org/10.1002/adma.201806236>.
- [8] Sarkar, A., Velasco, L., Wang, D., Wang, Q., Talasila, G., de Biasi, L., Kübel, C., Brezesinski, T., Bhattacharya, S.S., Hahn, H., & Breitung, B. (2018). High entropy oxides for reversible energy storage. [10.1038/s41467-018-05774-5](https://doi.org/10.1038/s41467-018-05774-5).
- [9] A.J. Wright, Q. Wang, C. Huang, A. Nieto, R. Chen, J. Luo, From high-entropy ceramics to compositionally-complex ceramics: a case study of fluorite oxides,

- J. Eur. Ceram. Soc. 40 (5) (2020) 2120–2129, <https://doi.org/10.1016/j.jeurceramsoc.2020.01.015>.
- [10] G. Anand, A.P. Wynn, C.M. Handley, C.L. Freeman, Phase stability and distortion in high-entropy oxides, *Acta Mater.* 146 (2018) 119–125, <https://doi.org/10.1016/j.actamat.2017.12.037>.
- [11] B.L. Musicó, D. Gilbert, T.Z. Ward, K. Page, E. George, J. Yan, D. Mandrus, V. Keppens, The emergent field of high entropy oxides: design, prospects, challenges, and opportunities for tailoring material properties, *APL Mater.* 8 (4) (2020) 040912, <https://doi.org/10.1063/5.0003149>.
- [12] A. Sarkar, B. Breitung, H. Hahn, High entropy oxides: the role of entropy, enthalpy and synergy, *Scr. Mater.* 187 (2020) 43–48, <https://doi.org/10.1016/j.scriptamat.2020.05.019>.
- [13] A.J. Wright, J. Luo, A step forward from high-entropy ceramics to compositionally complex ceramics: a new perspective, *J. Mater. Sci.* 55 (23) (2020) 9812–9827, <https://doi.org/10.1007/s10853-020-04583-W>. 2020 55:23.
- [14] S.J. McCormack, A. Navrotsky, Thermodynamics of high entropy oxides, *Acta Mater.* 202 (2021) 1–21, <https://doi.org/10.1016/j.actamat.2020.10.043>.
- [15] C.M. Rost, E. Sachet, T. Borman, A. Moballeghe, E.C. Dickey, D. Hou, J.L. Jones, S. Curtarolo, J.P. Maria, Entropy-stabilized oxides, *Nat. Commun.* 6 (2015), <https://doi.org/10.1038/NCOMMS9485>.
- [16] C.M. Rost, Z. Rak, D.W. Brenner, J.P. Maria, Local structure of the  $\text{Mg}_{x}\text{Ni}_{x}\text{Co}_{x}\text{Cu}_{x}\text{Zn}_{x}\text{O}(x=0.2)$  entropy-stabilized oxide: an EXAFS study, *J. Am. Ceram. Soc.* 100 (6) (2017) 2732–2738, <https://doi.org/10.1111/JACE.14756>.
- [17] C.M. Rost, Z. Rak, D.W. Brenner, J.P. Maria, Local structure of the  $\text{Mg}_{x}\text{Ni}_{x}\text{Co}_{x}\text{Cu}_{x}\text{Zn}_{x}\text{O}(x=0.2)$  entropy-stabilized oxide: an EXAFS study, *J. Am. Ceram. Soc.* 100 (6) (2017) 2732–2738, <https://doi.org/10.1111/jace.14756>.
- [18] Lower, S. (2023). Chem1 Virtual Textbook, Open Education Resource LibreTexts Project.
- [19] Navrotsky, A., Dorogova, M., Hellman, F., Cooke, D.W., Zink, B.L., Leshar, C.E., Boerio-Goates, J., Woodfield, B.F., & Lang, B. (2007). Application of calorimetry on a chip to high-pressure materials. doi: 10.1073/pnas.0608165104.
- [20] A. Sallian, S. Mandal, Entropy stabilized multicomponent oxides with diverse functionality—a review, in: *Critical Reviews in Solid State and Materials Sciences*, 47, Taylor and Francis Ltd, 2022, pp. 142–193.
- [21] Elliott, J.R.; Lira, C.T. (2012). Introductory chemical engineering thermodynamics. Page 604, Section 11.4.
- [22] Reference: De Hoff, R. (2006). Thermodynamics in materials science 2nd Edition, Page 226–227, Section 8.5.
- [23] A. Harari, J.P. Bocquet, M. Huber, R. Collongues, Crystal structure of the mixed oxide  $\text{HfTiO}_4$ , C. R. Hebd. Seances Acad. Sci. Ser. C 267 (20) (2003) 1316–1318.
- [24] R.E. Newnham, Crystal structure of  $\text{ZrTiO}_4$ , *J. Am. Ceram. Soc.* 50 (4) (1967), <https://doi.org/10.1111/J.1151-2916.1967.TB15085.X>, 216–216.
- [25] Aamlid, S.S., Johnstone, G.H.J., Mugeranza, S., Oudah, M., Rottler, J., & Hallas, A. M. (2023). Phase stability of entropy stabilized oxides with the  $\alpha\text{-PbO}_2$  structure.
- [26] F.H. Simpson, High Temperature Structural Ceramics, *Mater. Des. Eng.* (1960) 52.
- [27] R. Ruh, G.W. Hollenberg, E.G. Charles, V.A. Patel, Phase relations and thermal expansion in the system  $\text{HfO}_2\text{-TiO}_2$ , *J. Am. Ceram. Soc.* 59 (11–12) (1976) 495–499, <https://doi.org/10.1111/J.1151-2916.1976.TB09416.X>.
- [28] K.S. Mazdiyasi, L.M. Brown, Preparation and characterization of high-purity  $\text{HfTiO}_4$ , *J. Am. Ceram. Soc.* 53 (11) (1970) 585–589, <https://doi.org/10.1111/J.1151-2916.1970.TB15977.X>.
- [29] J.P. Coutures, J. Coutures, The system  $\text{HfO}_2\text{-TiO}_2$ , *J. Am. Ceram. Soc.* (1987) 70–76, <https://doi.org/10.1111/j.1151-2916.1987.tb05655.x>.
- [30] R.G. Hoagland, C.W. Marschall, A.R. Rosenfield, G. Hollenberg, R. Ruh, Microstructural factors influencing fracture toughness of hafnium titanate, *Mater. Sci. Eng.* 15 (1) (1974) 51–62, [https://doi.org/10.1016/0025-5416\(74\)90029-9](https://doi.org/10.1016/0025-5416(74)90029-9).
- [31] F. Canadieu, Characterization of Some Materials in the  $\text{HfO}_2\text{-TiO}_2$  System, 13, High-Temp-High Press, 1981, 97–97.
- [32] G. Bayer, M. Hofmann, L.J. Gauckler, Effect of ionic substitution on the thermal expansion of  $\text{ZrTiO}_4$ , *J. Am. Ceram. Soc.* 74 (9) (1991) 2205–2208, <https://doi.org/10.1111/J.1151-2916.1991.TB08285.X>.
- [33] G. Panneerselvam, R. Venkata Krishnan, K. Ananthasivan, M.P. Antony, Thermophysical properties of hafnium titanate, *Ceram. Int.* 38 (6) (2012) 5219–5222, <https://doi.org/10.1016/J.CERAMINT.2012.03.029>.
- [34] Lynch, R.W., & Morosin, B. (1972). Thermal expansion, compressibility, and polymorphism in hafnium and zirconium titanates. 10.1111/j.1151-2916.1972.tb11323.x.
- [35] H. Ikawa, A. Iwai, K. Hiruta, H. Shimojima, K. Urabe, S. Udagawa, Phase transformation and thermal expansion of zirconium and hafnium titanates and their solid solutions, *J. Am. Ceram. Soc.* 71 (2) (1988) 120–127, <https://doi.org/10.1111/J.1151-2916.1988.TB05827.X>.
- [36] S.J. McCormack, W.A. Wheeler, B.S. Hulbert, W.M. Kriven, Directions of zero thermal expansion and the peritectic transformation in  $\text{HfTiO}_4$ , *Acta Mater.* 200 (2020) 187–199, <https://doi.org/10.1016/j.actamat.2020.08.060>.
- [37] K. Honda, A. Sakai, M. Sakashita, H. Ikeda, S. Zaima, Y. Yasuda, Pulsed laser deposition and analysis for structural and electrical properties, of  $\text{HfO}_2\text{-TiO}_2$  composite films, *Jpn. J. Appl. Phys.* 43 (2004) [4A] 1571–6.
- [38] F. Chen, X. Bin, C. Hella, X. Shi, W.L. Gladfelter, S.A. Campbell, A study of mixtures of  $\text{HfO}_2$  and  $\text{TiO}_2$  as high-k gate dielectrics, *Microelectron. Eng.* 72 (1–4) (2004) 263–266, <https://doi.org/10.1016/j.mee.2004.01.001>.
- [39] M. Li, Z. Zhang, S.A. Campbell, H.J. Li, J.J. Peterson, Hafnium titanate as a high permittivity gate insulator: electrical and physical characteristics and thermodynamic stability, *J. Appl. Phys.* 101 (2007), 044509-1–9.
- [40] M. Li, Z. Zhang, S.A. Campbell, W.L. Gladfelter, M.P. Agustín, D.O. Klenov, S. Stemmer, Electrical and material characterizations of high-permittivity  $\text{HfTi}_{1-x}\text{O}_2$  gate insulators, *J. Appl. Phys.* 98 (2005), 054506-1–8.
- [41] G. Wolfram, H.E. Göbel, Existence range, structural and dielectric properties of  $\text{Zr}_x\text{Ti}_y\text{Sn}_z\text{O}_4$  ceramics ( $X + Y + Z = 2$ ), *Mater. Res. Bull.* 16 (1981) 1455–1463.
- [42] A. Bianco, G. Gusmano, R. Freer, P. Smith, Zirconium titanate microwave dielectrics prepared via polymeric precursor route, *J. Eur. Ceram. Soc.* 19 (1999) 959–963.
- [43] R. Christoffersen, P.K. Davies, Structure of commensurate and incommensurate ordered phases in the system  $\text{ZrTiO}_4\text{-Zr}_5\text{Ti}_7\text{O}_{24}$ , *J. Am. Ceram. Soc.* 75 (3) (1992) 563–569, <https://doi.org/10.1111/j.1151-2916.1992.tb07843.x>.
- [44] A.E. McHale, R.S. Roth, Low-temperature phase relationships in the system  $\text{ZrO}_2\text{-TiO}_2$ , *J. Am. Ceram. Soc.* 69 (11) (1986) 827–832, <https://doi.org/10.1111/j.1151-2916.1986.tb07368.x>.
- [45] P. Bordet, A. Mchale, A. Santoro, R.S. Roth, Powder neutron diffraction study of  $\text{ZrTiO}_4$ ,  $\text{Zr}_5\text{Ti}_7\text{O}_{24}$ , and  $\text{FeNb}_2\text{O}_7$ , *J. Solid-State Chem.* 64 (1986).
- [46] I. Saenko, M. Ilavskaja, G. Savinykh, O. Fabrichnaya, Experimental investigation of phase relations and thermodynamic properties in the  $\text{ZrO}_2\text{-TiO}_2$  system, *J. Am. Ceram. Soc.* 101 (1) (2018) 386–399, <https://doi.org/10.1111/jace.15176>.
- [47] R. Christoffersen, P.K. Davies, Extended defect intergrowths in  $\text{Zr}_x\text{Ti}_{1-x}\text{O}_4$ , *Solid State Ion.* 57 (1992).
- [48] E. López-López, C. Baudin, R. Moreno, I. Santacruz, L. Leon-Reina, M.A.G. Aranda, Structural characterization of bulk  $\text{ZrTiO}_4$  and its potential for thermal shock applications, *J. Eur. Ceram. Soc.* 32 (2) (2012) 299–306.
- [49] F. Azough, R. Freer, C.L. Wang, G.W. Lorimer, The relationship between the microstructure and microwave dielectric properties of zirconium titanate ceramics, *J. Mater. Sci.* 31 (1996).
- [50] Y.K. Kim, H.M. Jang, Lattice contraction and cation ordering of  $\text{ZrTiO}_4$  in the normal-to-incommensurate phase transition, *J. Appl. Phys.* 89 (11 D) (2001) 6349–6355.
- [51] A.E. McHale, R.S. Roth, Investigation of the phase transition in  $\text{ZrTiO}_4$  and  $\text{ZrTiO}_4\text{-SnO}_2$  solid solutions, *J. Am. Ceram. Soc.* 66 (2) (1983), C-18-C-20.
- [52] A. Yamamoto, T. Yamada, H. Ikawa, O. Fukunaga, K. Tanaka, F. Marumo, Modulated structure of zirconium titanate, *Acta Crystallogr. Sect. C Cryst. Struct. Commun.* 47 (8) (1991) 1588–1591.
- [53] G.D. Wilk, R.M. Wallace, J.M. Anthony, High-k gate dielectrics: current status and materials properties considerations, *J. Appl. Phys.* 89 (2001) 5243.
- [54] J. Domaradzki, D. Kaczmarek, A. Borkowska, M. Wolczyk, B. Paszkiewicz, Electrical properties of nanocrystalline  $\text{HfTiO}_4$  gate insulator, *Phys. Status Solidi A* (2006), 203 [9]2215–8.
- [55] J. Domaradzki, D. Kaczmarek, E.L. Prociow, A. Borkowska, R. Kudrawiec, J. Misiewicz, D. Schmeiser, G. Beuckert, Characterization of nanocrystalline  $\text{TiO}_2\text{-HfO}_2$  thin films prepared by low pressure hot target reactive magnetron sputtering, *Surf. Coat. Technol.* 200 (2006) 6283–6287.
- [56] T. Kidchob, P. Falcaro, P. Schiavuta, S. Enzo, P. Innocenzi, Formation of monoclinic hafnium titanate thin films via the sol-gel method, *J. Am. Ceram. Soc.* 91 (7) (2008) 2112–2116, <https://doi.org/10.1111/j.1551-2916.2008.02426.x>.
- [57] B.K. Hom, R. Stevens, B.F. Woodfield, J. Boerio-Goates, R.L. Putnam, K.B. Helean, A. Navrotsky, R.L. Putnam, The thermodynamics of formation, molar heat capacity, and thermodynamic functions of  $\text{ZrTiO}_4(\text{cr})$ , *J. Chem. Thermodyn.* 33 (2) (2001) 165–178, <https://doi.org/10.1006/JCHT.2000.0755>.
- [58] M. Brahlék, M. Gazda, V. Keppens, A.R. Zayza, S.J. McCormack, A. Mielewicz-Gryń, B. Musicó, K. Page, C.M. Rost, S.B. Sinnott, C. Toher, T.Z. Ward, A. Yamamoto, What is in a name: defining “high entropy” oxides, *APL Mater.* 10 (11) (2022).
- [59] Lee, T.A., Navrotsky, A., & Molodetsky, I. (2003). Enthalpy of formation of cubic yttria-stabilized zirconia.
- [60] T.A. Lee, A. Navrotsky, Enthalpy of formation of cubic yttria-stabilized hafnia, *J. Mater. Res.* 19 (6) (2004) 1855–1861, <https://doi.org/10.1557/JMR.2004.0234>.
- [61] W. Chen, T.A. Lee, A. Navrotsky, Enthalpy of formation of yttria-doped ceria, *J. Mater. Res.* 20 (1) (2005) 144–150, <https://doi.org/10.1557/JMR.2005.0017>.
- [62] S. Mukherjee, H. Ganegoda, A. Kumar, S. Pal, C.U. Segre, D.D. Sarma, Evolution of the Local Structure within Chromophoric Mn-O5 Trigonal Bipyramids in  $\text{Ym}_{1-x}\text{In}_x\text{O}_3$  with Composition, *Inorg. Chem.* 57 (15) (2018) 9012–9019, <https://doi.org/10.1021/acs.inorgchem.8b00997>.
- [63] G.C. Lau, T.M. McQueen, Q. Huang, H.W. Zandbergen, R.J. Cava, Long- and short-range order in stuffed titanate pyrochlores, *J. Solid State Chem.* 181 (1) (2008) 45–50, <https://doi.org/10.1016/j.jssc.2007.10.025>.
- [64] E.C. O’Quinn, J. Shamblyn, B. Perlov, R.C. Ewing, J. Neuefeind, M. Feygenson, I. Gussev, M. Lang, Inversion in  $\text{Mg}_{1-x}\text{Ni}_x\text{Al}_2\text{O}_4$  Spinel: new Insight into Local Structure, *J. Am. Chem. Soc.* 139 (30) (2017) 10395–10402, <https://doi.org/10.1021/jacs.7b04370>.
- [65] Gulgun, M.A., Kriven, W.M., & Nguyen, M.H. (1999). Processes for preparing mixed metal oxide powders.
- [66] Nguyen, M.H., Lee, S.J., & Kriven, W.M. (1999). Synthesis of oxide powders by way of a polymeric steric entrapment precursor route.
- [67] M.H. Nguyen, S.J. Lee, W.M. Kriven, Synthesis of oxide powders by way of a polymeric steric entrapment precursor route, *J. Mater. Res.* 14 (8) (1999) 3417–3426, <https://doi.org/10.1557/JMR.1999.0462>.
- [68] H.M. Rietveld, A profile refinement method for nuclear and magnetic structures, *J. Appl. Crystallogr.* 2 (2) (1969) 65–71, <https://doi.org/10.1107/S0021889869006558>.
- [69] B.H. Toby, R.B. Von Dreele, GSAS-II: the genesis of a modern open-source all purpose crystallography software package, *J. Appl. Crystallogr.* 46 (2) (2013) 544–549, <https://doi.org/10.1107/S0021889813003531>.
- [70] A. Navrotsky, Progress and new directions in high temperature calorimetry, *Phys. Chem. Miner.* 2 (1977) 89–104.
- [71] A. Navrotsky, Progress and new directions in high temperature calorimetry revisited, *Phys. Chem. Miner.* 24 (1997) 222–241.

- [72] A. Navrotsky, O.J. Kleppa, A calorimetric study of molten Na<sub>2</sub>MoO<sub>4</sub>-MoO<sub>3</sub> mixtures at 9700K, *Inorg. Chem.* 6 (11) (1967) 2119–2121, <https://doi.org/10.1021/IC50057A047/ASSET/IC50057A047.FP.PNG.V03>.
- [73] A.J. Kropf, J. Katsoudas, S. Chattopadhyay, T. Shibata, E.A. Lang, V.N. Zyryanov, B. Ravel, K. Mcivor, K.M. Kemner, K.G. Scheckel, S.R. Bare, J. Terry, S.D. Kelly, B. A. Bunker, C.U. Segre, The new MRCAT (Sector 10) bending magnet beamline at the advanced photon source, *AIP Conf. Proc.* 1234 (2010) 299–302, <https://doi.org/10.1063/1.3463194>.
- [74] M. Newville, IFEFFIT: interactive XAFS analysis and FEFF fitting, *J. Synchrotron Radiat.* (2001). <http://astro.caltech.edu/>.
- [75] B. Ravel, M. Newville, Synchrotron radiation athena, artemis, hephaestus: data analysis for X-ray absorption spectroscopy using IFEFFIT, *J. Synchrotron Radiat.* 12 (2005) 537–541, <https://doi.org/10.1107/S0909049505012719>.
- [76] M.W. Chase Jr, NIST-JANAF Thermochemical Tables, Fourth Edition, *J. Phys. Chem. Ref. Data Monogr.* 9 (1998) 1–1951.
- [77] E.J. Huber, C.E. Holley, Enthalpy of Formation of Hafnium Dioxide Energy, *J. Chem. Eng. Data* 13 (1967) 252–253.
- [78] H.K. Hardy, A “sub-regular” solution model and its application to some binary alloy systems, *Acta Metall.* 1 (2) (1953) 202–209, [https://doi.org/10.1016/0001-6160\(53\)90059-5](https://doi.org/10.1016/0001-6160(53)90059-5).
- [79] D.C. Koningsberger, R. Prins, EXAFS determination of short range order and local structures in materials, *TrAC Trends Anal. Chem.* 1 (1) (1981) 16–21. Pages.
- [80] A. Mesquita, A. Michalowicz, V.R. Mastelaro, XANES measurements probing the local order and electronic structure of Pb<sub>1-x</sub>BaxZr<sub>0.40</sub>Ti<sub>0.60</sub>O<sub>3</sub> ferroelectric materials, *J. Alloys Compd.* 640 (2015) 355–361.
- [81] M.U. González-Rivas, S.S. Aamlid, M.R. Rutherford, J. Freese, R. Sutarro, N. Chen, E.E. Villalobos-Portillo, H. Castillo-Michel, M. Kim, H. Takagi, R.J. Green, A. M. Hallas, Impact of synthesis method on the structure and function of high entropy oxides, *J. Am. Chem. Soc.* (2024), <https://doi.org/10.1021/JACS.4C05951>.